

Infrared ellipsometry study of the charge dynamics in K_3p -terphenyl

Qi He^{1,*}, P. Marsik¹, F. Le Mardelé¹, B. Xu¹, M. Sharma², N. Pinto^{2,3}, A. Perali⁴,
C. Di Nicola⁵, C. Pettinari⁵, D. Baeriswyl¹ and C. Bernhard^{1,†}

¹Department of Physics, University of Fribourg, 1700 Fribourg, Switzerland

²School of Science and Technology, Physics Division, University of Camerino, 62032 Camerino, Italy

³Advanced Materials Metrology and Life Science Division, INRiM, 10135 Torino, Italy

⁴School of Pharmacy, Physics Unit, University of Camerino, 62032 Camerino, Italy

⁵School of Science and Technology, Chemistry Division, University of Camerino, 62032 Camerino, Italy



(Received 9 January 2023; accepted 21 March 2023; published xxxxxxxxx)

We report an infrared ellipsometry study of the charge carrier dynamics in polycrystalline K_xp -terphenyl samples with nominal $x = 3$, for which signatures of high-temperature superconductivity were previously reported. The infrared spectra are dominated by two Lorentzian bands with maxima around 4000 and 12 000 cm^{-1} which, from a comparison with calculations based on a Hückel model, are assigned to intramolecular excitations of π electrons of the anionic p -terphenyl molecules. The intermolecular electronic excitations are much weaker and give rise to a Drude peak and a similarly weak Lorentzian band around 220 cm^{-1} . A dc resistivity of about 0.3 $\Omega \text{ cm}$ at 300 K is deduced from the IR data, comparable to values measured by electrical resistivity on a twin sample. The analysis of the temperature dependence of the low-frequency response reveals a gradual decrease of the plasma frequency and the scattering rate of the Drude peak below 300 K that gets anomalously enhanced below 90 K. The corresponding missing spectral weight of the Drude peak appears blueshifted towards the Lorentz band at 220 cm^{-1} . This characteristic blueshift signifies an enhanced localization of the charge carriers at low temperatures and contrasts the behavior expected for a bulk superconducting state for which the missing spectral weight would be redshifted to a delta function at zero frequency that accounts for the loss-free response of the superconducting condensate. Our data might still be compatible with a filamentary superconducting state with a volume fraction well below the percolation limit for which the spatial confinement of the condensate can result in a plasmonic resonance at finite frequency.

DOI: 10.1103/PhysRevB.00.004500

I. INTRODUCTION

Organic molecular solids have long been understood as insulators. This changed in the 1970s and early 1980s with the synthesis of conducting charge-transfer salts, such as tetrathiofulvalinium tetracyanoquinodimethane (TTF TCNQ) [1–3] and (TMTSF)₂PF₆ [4]. In these materials, reviewed in Ref. [5], the relatively strong overlap between electronic wave functions due to the face-to-face packing of molecules leads to one-dimensional bands close to the Fermi energy along the stacks. The Bechgaard salts (TMTSF)₂X, where $X = \text{PF}_6$, ClO_4 , etc., show a variety of phases, including spin-density waves, charge order, and, in particular, superconductivity [6,7]. The possibility of superconductivity in a one-dimensional organic metal, possibly even up to high temperatures, had been theoretically proposed already in 1964 by Little [8]. Such an organic high- T_c superconductor would enable a wide range of promising applications for biological devices, photovoltaics (solar cells), memory materials, optoelectronic devices, and other advanced technologies.

The critical temperatures of superconducting Bechgaard salts are low, of the order of 1 K. Higher T_c 's were reached in the quasi-two-dimensional organic compounds (BEDT-TTF)₂X [9], up to 14.2 K [10]. These materials exhibit a variety of exotic phases, from spin liquids to unconventional superconductivity [11–13].

The discovery of C₆₀ (sometimes simply called fullerene) in 1985 marked the beginning of a new era in the research on organic molecular compounds [14]. Solid C₆₀ is a cubic material and therefore quite different from the quasi-one- and quasi-two-dimensional charge transfer salts mentioned above. The intermolecular overlap is very small in all directions (and not only between chains as in TTF TCNQ or between planes as in graphite) and therefore the molecular orbitals are good starting points for describing electronic bands in solid C₆₀ [15]. In this sense the fullerenes are quasi-zero-dimensional. Solid C₆₀ is semiconducting, with an optical gap of about 2 eV [16]. Doping with potassium renders the material metallic and even superconducting, with $T_c = 18$ K for K₃C₆₀ [17]. At present, the commonly accepted record value for an organic superconductor of $T_c = 38$ K is held by Cs₃C₆₀ under high pressure [18]. It seems to be widely accepted that the threefold degeneracy of the lowest unoccupied molecular orbital (LUMO) plays an important role in the superconductivity of alkali-metal-doped fullerene, through the enhancement of the

*qi.he@unifr.ch

†christian.bernhard@unifr.ch

electron-phonon coupling by the Jahn-Teller effect [19], but electron correlation effects clearly are also relevant, especially for Cs_3C_{60} , a Mott insulator under ambient pressure [20]. Superconductivity in fcc compounds, such as K_3C_{60} , Rb_3C_{60} , or $\text{Rb}_2\text{KC}_{60}$, appears to be quite distinct from that observed in the A15 compound Cs_3C_{60} . In fact, T_c decreases with chemical [19] or physical pressure [21] in the former materials, while Cs_3C_{60} exhibits a dome-like shape [18]. An interesting question is also the role of stoichiometry. Experimental studies consistently indicate that the critical temperature has a maximum at half filling, i.e., for three electrons added to the LUMO [22–25].

In 2010, superconductivity was reported for the first time in a polycyclic aromatic hydrocarbon, namely, pice (C₂₂H₁₄) doped with potassium [26,27], with a surprisingly large critical temperature, $T_c = 18$ K. Since then, other materials of the same type have been found to become superconducting by doping, notably phenanthrene (C₁₄H₁₀) with $T_c = 5$ K [28], dibenzopentacene (C₃₀H₁₈) with $T_c = 33$ K [29], and pentacene (C₂₂H₁₄) with $T_c = 4.5$ K [30]. The interpretation of some of these experiments has been questioned [31]. In fact, there are problems with hydrocarbon superconductors [27], for instance the shielding fraction obtained from the magnetization is very low, typically of the order of 1%.

More recently, evidence of superconductivity has also been reported for several members of the family of paralogophenyls, e.g., in K_3p -quinquephenyl (C₃₀H₂₂) with $T_c = 7.3$ K [32], in K-doped quaterphenyl [33], and in K-doped biphenyl (C₁₂H₁₀) with $T_c = 7.2$ K [34]. The signatures of even higher T_c values of 43 K or even up to 123 K have been reported for p -terphenyl (C₁₈H₁₄) doped with potassium, with a nominal K content of $x = 3$ [35–37]. Evidence for a superconducting transition has been reported here mainly from magnetic susceptibility measurements. The analysis of the magnetic susceptibility data, however, yields a small superconducting volume fraction on the order of only a few percent. This latter result has been confirmed by a magnetization study of an independent group on polycrystalline K_3p -terphenyl samples that were synthesized under high pressure conditions [38]. Meanwhile, gap-like features in the electronic excitation spectrum that are reminiscent of a superconducting order have been observed with angle-resolved photoemission spectroscopy [39] and with scanning tunneling spectroscopy [40] on the surface of p -terphenyl crystals on which monolayers of potassium have been evaporated under ultrahigh vacuum condition. Signatures of a possible high- T_c superconducting phase have also been reported by electrical measurements [41]. The nominal composition of the bulk samples for which signatures of high- T_c superconductivity have been reported amounts to K_3p -terphenyl [36]. Nevertheless, it remains disputed whether in these samples the potassium is homogeneously distributed. Accordingly, the superconducting phase might have a different K content or even originate from clusters of K-rich material for which the composition is presently unknown as discussed, e.g., in Refs. [42–44]. Moreover, the high sensitivity of the $\text{K}_x p$ -terphenyl (KPT) samples to oxygen and moisture causes them to decompose rather rapidly under ambient conditions. This makes it quite difficult to study, for example with infrared spectroscopy, their bulklike free carrier

response and the signatures of a possible superconducting state.

The infrared spectroscopy technique probes the complex dielectric function of a material and thus provides valuable information about the dynamics of the mobile or weakly bound charge carriers as well as about their interband transitions and the related band structure [45,46]. In organic conductors the low-energy electronic response is typically governed by the intermolecular excitations for which the magnitude depends on the stacking and the bonding between the molecules and thus can be strongly anisotropic and exhibit large variations between different materials. The response at higher energy and the band gaps are typically characteristic of the intramolecular excitations of the individual molecules and thus can serve as “fingerprints” of their structure and their ionization level. Prominent examples of materials for which these electronic properties have been extensively studied with infrared spectroscopy are the Bechgaard salts, like (TMTSF)₂AsF₆ [47] and k-(BEDT-TTF)₂X [48–52] or the doped fullerenes [16].

Especially powerful is the spectroscopic ellipsometry technique which measures the change of the polarization state of the light upon reflection from the sample surface, rather than the intensity. It provides direct access to the real and the imaginary parts of the dielectric function of a given material [53,54]. Unlike the conventional reflection technique, it does not require reference measurements which are typically done by replacing the sample with a reference mirror or by gold coating the sample surface, nor does it require a Kramers-Kronig transformation, for which the measured data have to be extrapolated toward zero and infinite frequency. The ellipsometry technique is therefore well suited to measure the dielectric function of samples that have to remain under inert gas atmosphere or very high vacuum condition, before and during the measurements, and therefore are sealed in a closed cell with suitable windows for the optical access for which it is difficult to perform accurate reference measurements. Ellipsometry is commonly applied in the near-infrared, visible, and UV ranges, where ellipsometers are commercially available. Meanwhile, some groups, including ours, have built ellipsometers that operate in the far-infrared [55,56] and the terahertz ranges [57–59] and used them to study the electronic properties of various insulators, semiconductors, metals, and even superconductors, including organic materials [60].

In the following we present an infrared ellipsometry study of a polycrystalline sample of heavily K-doped p -terphenyl that decomposes rapidly under ambient condition and thus needs to be handled and measured under dry inert gas atmosphere or under high vacuum. For this purpose we have equipped our infrared ellipsometer with an optical cell which has windows made from undoped silicon (or alternatively from KBr) that provide optical access to the sample and enable ellipsometry measurements. In detail, in Sec. II, we provide the technical details about the sample preparation and the ellipsometry and electronic transport experiments. In Sec. III, we discuss the infrared data and analyze them in terms of a simple model, with a Drude part and several Lorentz oscillators. In Sec. IV, the main absorption peaks are attributed to intramolecular excitations and interpreted semi-quantitatively, according to Hückel theory. Intermolecular

excitations are made responsible for the weak low-frequency absorption. Section V presents the temperature dependence of both the low-frequency optical conductivity and the electrical resistivity. The observed spectral weight loss of the Drude peak is consistent with the upturn of resistivity at low temperatures. Our main findings and conclusions are summarized in Sec. VI. Finally, the Appendix presents details about orbitals and optical transitions of the *p*-terphenyl molecule, within Hückel's tight-binding approximation.

II. EXPERIMENTAL PROCEDURE

Polycrystalline potassium doped *p*-terphenyl, KPT, was synthesized at the University of Camerino, as described in Ref. [41]. Inside a glovebox, the potassium was cut in little pieces and mixed with the *p*-terphenyl in a molar ratio of 3:1 as to achieve a nominal composition of $x = 3$. To enable the chemical reaction, the mixture was sealed in a glass tube under argon atmosphere and heated to a temperature of 503 K at which it was kept for 2 h. The resulting black powder, very sensitive to oxygen and water, was kept under dry and inert atmosphere of pure argon gas.

Temperature-dependent electrical resistivity and current-voltage *I*-*V* characteristics were carried out on compressed KPT powder. A redesigned sample holder, with respect to those used in Ref. [41], was fabricated and used in this paper. The sample holder consists in a Teflon cylinder of 12 mm of internal diameter, closed at the two ends by copper electrodes that are electrically insulated against each other. The cylinder was filled with 40 mg of KPT powder, under a dry Ar atmosphere, and pressure was applied to the two electrodes and kept during the measurement. For this paper, the powder was compressed at about 0.45 MPa, in all investigated samples. Resistivity and *I*-*V* characteristics were measured with a pulsed technique, sourcing short current pulses of 1.1 ms of duration, either fixed or with a varying intensity, by a Keysight source meter, model B2912A, in the four-wire geometry of contacts. Compared to the standard dc current technique, the pulsed one allows us to minimize thermal electromotive force offsets [61] and to source higher current intensities. No appreciable differences were detected in the electrical transport properties measured by the pulsed and constant dc current techniques, at low current density. The sample temperature has been detected with a calibrated Si diode thermometer (Lakeshore model DT-670).

For the optical measurements pellets with a diameter of 12 mm and a thickness of about 1 mm were pressed from the K_3p -terphenyl powder. Such pellets have been prepared from three different growth batches which all have the same nominal composition of K_3p -terphenyl. For sending the samples to the University of Fribourg, they were enclosed in sealed plastic containers filled with argon gas.

In Fribourg the containers were transferred to a glovebox filled with dry Ar gas where they were opened and the samples were mounted in a homemade optical cell. A schematic drawing and an image of this optical cell with a sample (black pellet) mounted are displayed in Fig. 1. The sample was glued to a copper holder with vacuum grease to enable a good thermal contact. The cell was sealed inside the glovebox under dry Ar gas atmosphere using viton o-rings. The optical

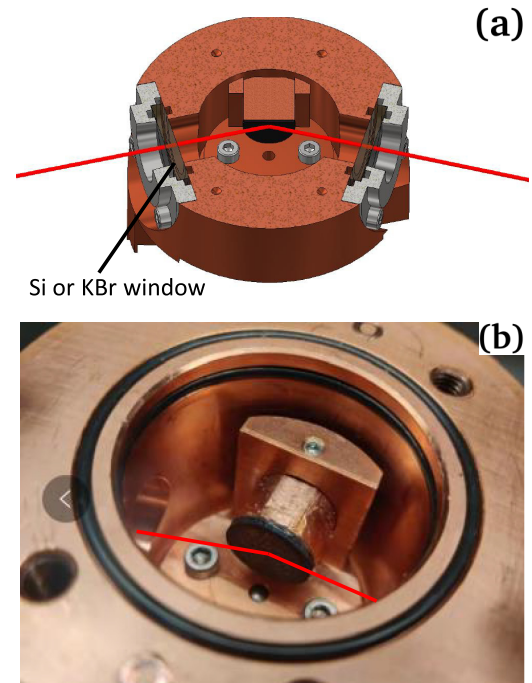


FIG. 1. (a) Schematic drawing of the cell for infrared ellipsometry measurements under dry and inert gas atmosphere. Red lines show the beam path of the incident and the reflected photons. (b) Photographic image of the inside of the cell with a K_3p -terphenyl sample (black pellet) mounted.

access for the ellipsometry measurements was enabled by two windows from pure silicon (sealed with viton rings) that are transparent in the entire infrared range up to 8000 cm^{-1} , except for a narrow region between 500 and 600 cm^{-1} with strong multiphonon absorption. Alternatively, we used KBr windows that are transparent from 350 cm^{-1} up to the UV range. Subsequently, the sealed optical cell with the sample inside was mounted on the cold head of a He-flow cryostat (from Cryovac) that enables temperatures ranging from 6 to 400 K. Our homebuilt infrared ellipsometer setup is attached to a fast Fourier transform infrared spectrometer (Bruker VERTEX 70 v). Its outline is described in Ref. [56]. The ellipsometric spectra have been recorded at an angle of incidence of $\phi = 75^\circ$ for the temperature range from 300 to 6 K. In the far-infrared range from about 50 to 700 cm^{-1} we used a rotating analyzer setup with polarizers made from wire grids that are evaporated on thin polyethylene foils. The midinfrared range from about 600 to 5000 cm^{-1} was measured with a rotating compensator setup based on a ZnSe prism and wire grid polarizers on KRS-5 substrates. For the near-infrared range from 5000 to $10\,000\text{ cm}^{-1}$ we used a rotating analyzer configuration with Glan-Thompson polarizers from Calcite. For the entire spectral range a He-cooled bolometer was used as detector.

III. ANALYSIS OF THE ROOM-TEMPERATURE SPECTRA

Figure 2(a) displays the spectrum at 300 K of the optical conductivity of a polycrystalline K_3p -terphenyl sample for the frequency range from about 50 to $10\,000\text{ cm}^{-1}$ (6 meV to 1.25 eV). Figure 2(b) shows a magnified view of the low-

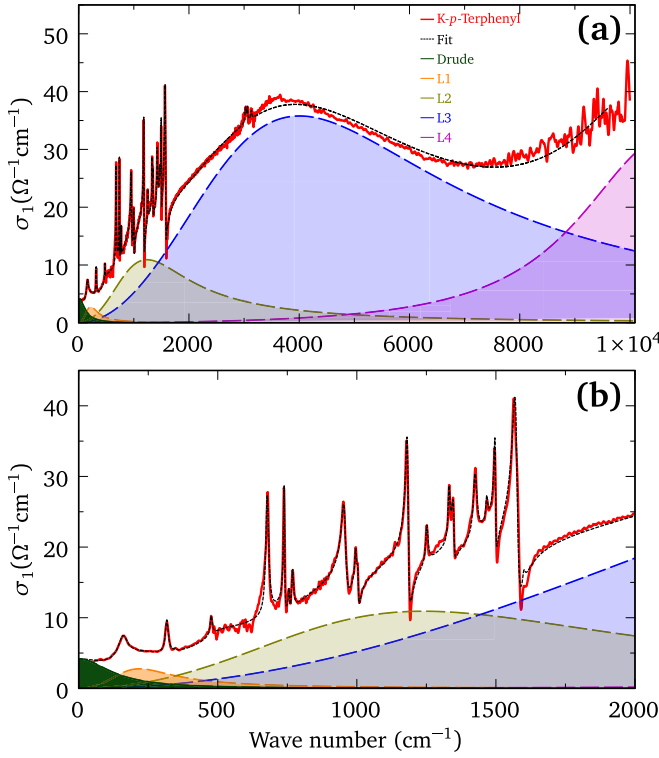


FIG. 2. (a) Broad-band spectrum of the optical conductivity at 300 K of polycrystalline K_3p -terphenyl. Solid lines and corresponding shaded areas show the contributions of the Drude peak (dark green) and of the broad Lorentz oscillators, as obtained with the fit function (1). (b) Magnified view of the low-frequency part of the optical conductivity spectrum.

frequency part of the spectrum up to 2000 cm^{-1} . Similar spectra have been obtained by samples belonging to three different growth batches of K_3p -terphenyl.

The electronic part of the spectrum of the complex dielectric function $\varepsilon(\omega)$ has been fitted to a Drude peak and four Lorentz oscillators:

$$\varepsilon(\omega) = \varepsilon_\infty - \frac{\omega_{p0}^2}{\omega^2 + i\omega\Gamma_0} + \sum_{i=1}^4 \frac{\omega_{pi}^2}{\omega_i^2 - \omega^2 - i\omega\Gamma_i}, \quad (1)$$

where ω_{p0} and Γ_0 are the plasma frequency and the scattering rate of the Drude model, respectively, ω_i is the eigenfrequency, Γ_i is the linewidth and ω_{pi} is the plasma frequency of the i th Lorentz oscillator, and ε_∞ is the high-frequency dielectric constant representing interband transitions well above the measured range. The individual contributions of the Drude and Lorentz oscillators are shown by solid lines and corresponding shadings. The parameters obtained from the fit are listed in Table I, which also shows the spectral weights of the Drude and Lorentz bands, defined as

$$W_{\text{spec}_i} \equiv \int_0^\infty \sigma_{1i}(\omega) d\omega = \frac{\pi}{2} \varepsilon_0 \omega_{pi}^2 = \frac{\pi N_i e^2}{2m_i}. \quad (2)$$

Here e is the electron charge, while m_i and N_i are, respectively, the effective mass and the density of electrons involved in the i th component of the spectrum.

TABLE I. Parameters of the Drude and Lorentz oscillators derived by fitting the infrared spectra of K_3p -terphenyl with Eq. (1). Units are cm^{-1} for ω_i , ω_{pi} , and Γ_i , and $\Omega^{-1} \text{ cm}^{-2}$ for the spectral weights W_{spec_i} .

Transition	ω_i	Γ_i	ω_{pi}	W_{spec_i}
Drude		311	247	1586
L_1	218	285	325	2746
L_2	1239	1793	1084	30551
L_3	4003	6199	3647	345815
L_4	10700	4015	2786	201807

Unfortunately, we could not extend the ellipsometry measurements to the range above $10\,000 \text{ cm}^{-1}$, to determine more accurately the center frequency and the spectral weight of the L_4 band. This is due to scattering and depolarization effects which appear if the wavelength of the photons reaches the grain size of the polycrystalline samples. Another problem is related to luminescence effects which become prominent as the photon energy approaches the band gap [62,63]. Nevertheless, since ellipsometry provides independent measures of the real and imaginary parts of the dielectric function (or related optical response functions), the data at hand allow us to obtain at least a rough estimate of the center frequency and the spectral weight of the L_4 band.

The infrared spectrum also contains several much narrower peaks, well fitted as (asymmetric) Lorentz oscillators (dashed lines in Fig. 2). We attribute them to infrared-active lattice vibrations (phonons). The individual contributions of these phonons are neither displayed in Fig. 2 nor discussed in this paper, in which the focus is on electronic excitations.

Figure 3 compares the infrared conductivity spectra of K_3p -terphenyl (red line) and a bare p -terphenyl sample (black line) at 300 K. The latter exhibits an insulatorlike response with a vanishing electronic conductivity, in good agreement with the reported band gap of about 3.5 eV [64]). In return, this confirms that the electronic conductivity of the K_3p -terphenyl sample originates from the electrons that are transferred from the K atoms to the π orbitals of the p -terphenyl molecules.

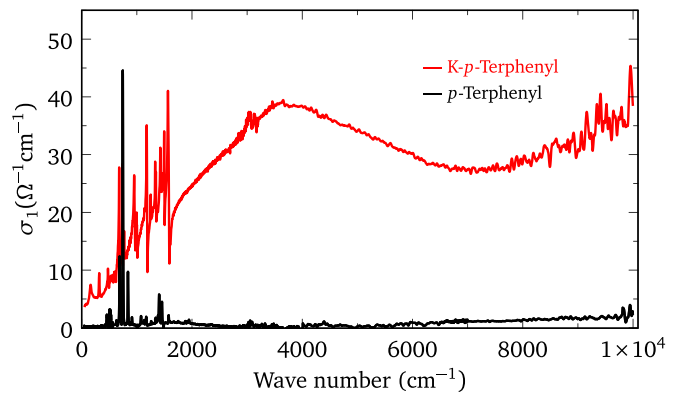


FIG. 3. Comparison of the optical conductivity spectra of polycrystalline samples of pristine p -terphenyl (black) and K_3p -terphenyl (red) at 300 K.

The total spectral weight of the Drude and Lorentz bands allows us to estimate the number of electrons participating in these transitions. Assuming a free-electron mass, $m_i = m_e$, we determine the number of carriers per p -terphenyl molecule, N_{eff} , through the equation

$$N_{\text{eff}} = \frac{N}{N_0} = \frac{1}{N_0} \frac{2m_e}{\pi e^2} W_{\text{spec, tot}}, \quad (3)$$

where N_0 is the volume density of p -terphenyl molecules (about $32.5 \times 10^{20} \text{ cm}^{-3}$). We obtain $N_{\text{eff}} \approx 0.09$. Considering a strong anisotropy of the intra- and intermolecular electronic excitations and assuming a powder average of randomly oriented grains that are smaller than the wavelength, this value corresponds to about 10% of the one expected for nominally three electrons per molecule. This discrepancy can be explained (at least partially) by the low volume density of the sample which has been pressed from powder, by an electron mass that exceeds m_e , and by the lack of an effective medium description that accounts for the shape of the crystallites and their particular electronic anisotropy (see, e.g., Ref. [65]). However, this discrepancy might also be an indication that the number of π electrons per molecule is somewhat less than the nominal three electrons.

The low-frequency part of the electronic conductivity spectrum contains a very weak Drude peak at the origin and the similarly weak Lorentzian mode L_1 . A linear extrapolation at 300 K towards zero frequency, or likewise the fitted parameters ω_{p0} and Γ_0 , yield a dc conductivity of about $4 \Omega^{-1} \text{ cm}^{-1}$ that matches reasonably well the dc resistivity measured on a pellet from the same growth batch. The spectral weight of the Drude peak is about two orders of magnitude lower than that of the L_3 band (see Table I). Such a small free carrier spectral weight is not uncommon for low-dimensional organic conductors for which the intermolecular hopping parameter is typically much smaller than the intramolecular ones [5,52]. We will come back to this point in Sec. IV.

IV. ASSIGNMENT OF THE MAIN TRANSITIONS

Hückel theory is quite useful for discussing qualitatively the optical spectra of organic molecular solids. This has been demonstrated in the case of C_{60} , where the discrete molecular energy levels are broadened into narrow bands [19] in such a way that the level structure of the molecule remains visible in the optical absorption spectrum of the molecular solid [16]. In Hückel's theory of conjugated hydrocarbons π electrons are treated explicitly, in tight-binding approximation, while σ electrons are taken into account through the elastic energy of bond stretching [66–68]. The hopping amplitudes are supposed to vary linearly with respect to changes in bond lengths around an average value t_0 , with a slope α . The elastic energy involved in bond stretching depends on a force constant K . The theory is worked out in detail for a p -terphenyl molecule in the Appendix, using parameters t_0 , α , and K extracted from electronic and vibrational properties of other molecules (such as benzene). Therefore we do not use any adjustable parameters. We should however keep in mind that the parametrization has been made for neutral molecules. Some modifications due to charge transfer have been discussed in the case of intercalated graphite [69], but

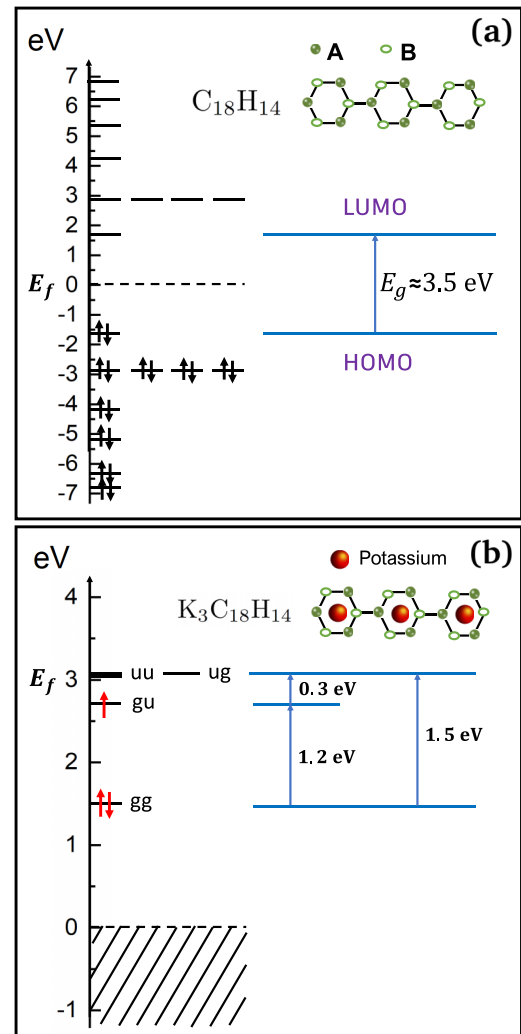


FIG. 4. Energy levels and lowest optical transitions according to the Hückel model. (a) Hypothetical case of pristine p -terphenyl with equal bond lengths. (b) K_3p -terphenyl for optimized bond lengths.

we leave the parameters t_0 , α , and K unchanged and limit ourselves to changes in the bond order (see the Appendix).

Figure 4(a) shows the energy levels of a neutral p -terphenyl molecule for the case of equal bond lengths. The spectrum has particle-hole symmetry, because the system is bipartite in tight-binding approximation, i.e., the sites can be subdivided into two sublattices A and B in such a way that hopping occurs only between the two sublattices, as illustrated in Fig. 4(a). The energy difference between the LUMO and the highest occupied orbital (HOMO) is about 3.5 eV, in good agreement with the energy gap reported for pristine p -terphenyl. In contrast to C_{60} , where the LUMO is threefold degenerate (even sixfold for equal bond lengths [70]), the LUMO (as well as the HOMO) is nondegenerate in the case of p -terphenyl. The next level (“Lumo+1”) is fourfold degenerate, but it is split (of the order of 20 meV) into two nondegenerate and one doubly degenerate level if the bond lengths are optimized. Much larger “polaronic” shifts (of the order of 0.3 eV) occur if we add electrons, as illustrated in Fig. 4(b) for the case of K_3p -terphenyl. We classify the orbitals according to

TABLE II. Low-energy intramolecular transitions of K_3p -terphenyl according to Hückel theory. The transition energies are given in units of eV, and the oscillator strengths are given in units of $\Omega^{-1} \text{ cm}^{-2}$.

Transition	Transition energy	Spectral weight
$gg \rightarrow gu$	1.232	1.396×10^6
$gg \rightarrow ug$	1.522	0.340×10^6
$gu \rightarrow uu^{(1)}$	0.287	8.369×10^6
$gu \rightarrow uu^{(2)}$	0.290	9.505×10^6

their parity with respect to reflections by the long and short axes. Thus gg means even (“gerade”) with respect to both reflections, gu means even with respect to the first reflection and odd (“ungerade”) with respect to the second reflection, and so on. Optical transitions are symmetry allowed for $gg \rightarrow gu$, $gg \rightarrow ug$, and $gu \rightarrow uu$, with transition energies as indicated in Fig. 4(b).

The optical conductivity can also be calculated in the framework of Hückel theory, as detailed in the Appendix. The symmetry of molecular orbitals implies selection rules, as expected, namely, the transition $gg \rightarrow gu$ occurs for light polarized parallel to the long axes, while the transitions $gg \rightarrow ug$ and $gu \rightarrow uu$ require the polarization to be parallel to the short axis. Since the experiments were performed on polycrystalline samples we have calculated the powder averaged response. The results are shown in Table II.

The predominant features of the electronic response of the K_3p -terphenyl sample are the Lorentzian modes L_3 and L_4 . We show now that they agree reasonably well with the transitions predicted by Hückel theory for a trianionic p -terphenyl molecule. The L_3 band with an eigenfrequency of $\omega_3 = 4000 \text{ cm}^{-1}$ (0.5 eV) can be roughly accounted for by the dipole-allowed $gu \rightarrow uu$ transitions around 0.3 eV (Fig. 4 and Table II). Likewise, the L_4 band with $\omega_4 = 12000 \text{ cm}^{-1}$ (1.5 eV) can be well described by the $gg \rightarrow gu$ and $gg \rightarrow ug$ transitions at 1.2 and 1.5 eV, respectively.

The relatively poor agreement between theory and experiment in the case of the L_3 transition (0.3 versus 0.5 eV) can be understood as follows. Electron-electron correlations are known to produce non-negligible effects both for the ground state and for the excited states of hydrocarbons [71]. Hückel theory also predicts a “bipolaronic” path for doping, as shown in the Appendix. If Coulomb repulsion among π electrons is taken explicitly into account, this scenario is not expected to be energetically favored.

The comparison of the spectral weights obtained from theory and experiment is more tricky. Clearly, the theoretical values of Table II are substantially larger than the experimental values of Table I. The discrepancy in the relative spectral weights is even more striking. While the experimental values for the L_3 mode are about 1.5 times larger than those for the L_4 mode, the theoretical numbers for the $gu \rightarrow uu$ transitions are an order of magnitude larger than those for the $gg \rightarrow gu$ and $gg \rightarrow ug$ transitions. The main difference between the two types of transitions is that the former depend strongly on the occupation of the level at 2.7 eV, while the latter are less sensitive. The agreement of the relative intensities thus could

be greatly improved by postulating that the actual charge per molecule is less than 3, due to either an only partial electron transfer from the K ions to the p -terphenyl molecules or a K concentration that is lower than the nominal one. Evidence for a lower effective electron doping has been also found from the experiments in Ref. [41] and the calculations in Ref. [44].

The corresponding intermolecular hopping is expected to be much weaker than the intramolecular one and will therefore mainly contribute to the broadening of the intramolecular levels as shown in Fig. 4 (in addition to defects and a possible variation of the local K content). Moreover, it accounts for the weak Drude peak that arises from the intermolecular excitations of the single electron in the gu level at 2.7 eV and likely also for the weak L_1 mode at 220 cm^{-1} . The latter could be explained by a variation of the local K content and the subsequent transfer of electrons to the p -terphenyl molecules, which would give rise to small changes of the intramolecular energy levels.

V. TEMPERATURE DEPENDENCE OF THE LOW-FREQUENCY RESPONSE

Next, we discuss the temperature dependence of the weak Drude peak and of the low-energy Lorentzian L_1 . Figures 5(a) and 5(b) show the measured spectra (symbols) of the real and imaginary parts of the dielectric function, ϵ_1 and ϵ_2 , up to 450 cm^{-1} at the highest and the lowest temperatures of 300 and 6 K, respectively. The black dashed line shows the best fit to the complex dielectric function in the range below 450 cm^{-1} using a Drude-Lorentz model similar to that of Eq. (1). The colored lines show the individual contributions of the Drude peak (blue), the L_1 (orange) and L_2 peaks (dark green), and the low-energy IR phonons (red). To minimize the number of fit parameters, we fixed the position and width of the L_1 peak as well as the position and weight of the L_2 peak at the values obtained at 300 K. The obtained temperature dependence of the plasma frequency and width of the Drude peak and the plasma frequency of the L_1 peak are displayed in Figs. 5(c) and 5(d). For the Drude response both the plasma frequency ω_{p0} and the scattering rate Γ_0 decrease substantially as the temperature is reduced below 300 K. Moreover, for both Drude parameters the temperature-dependent decrease appears to be anomalously enhanced below about 90 K. The plasma frequency of the L_1 peak is also temperature dependent and increases towards low temperature. Notably, the spectral weight loss of the Drude peak between 90 and 6 K of about $228 \Omega^{-1} \text{ cm}^{-2}$ matches rather well the corresponding spectral weight gain of the L_1 peak which amounts to about $244 \Omega^{-1} \text{ cm}^{-2}$. Overall, the fitting of the low-energy response provides evidence for a low concentration of mobile carriers that tend to get localized as the temperature is decreased. Why this localization is anomalously enhanced below about 90 K remains to be understood.

We now turn to the comparison of the charge transport, as determined from the infrared spectra and the resistivity data. Figure 6(a) shows the temperature dependence of the inverse dc conductivity, derived from the fit parameters ω_{0D} and Γ_D of the Drude peak.

The temperature-dependent electrical resistivity, $\rho(T)$, has been detected in a twin K_3p -terphenyl sample and is displayed

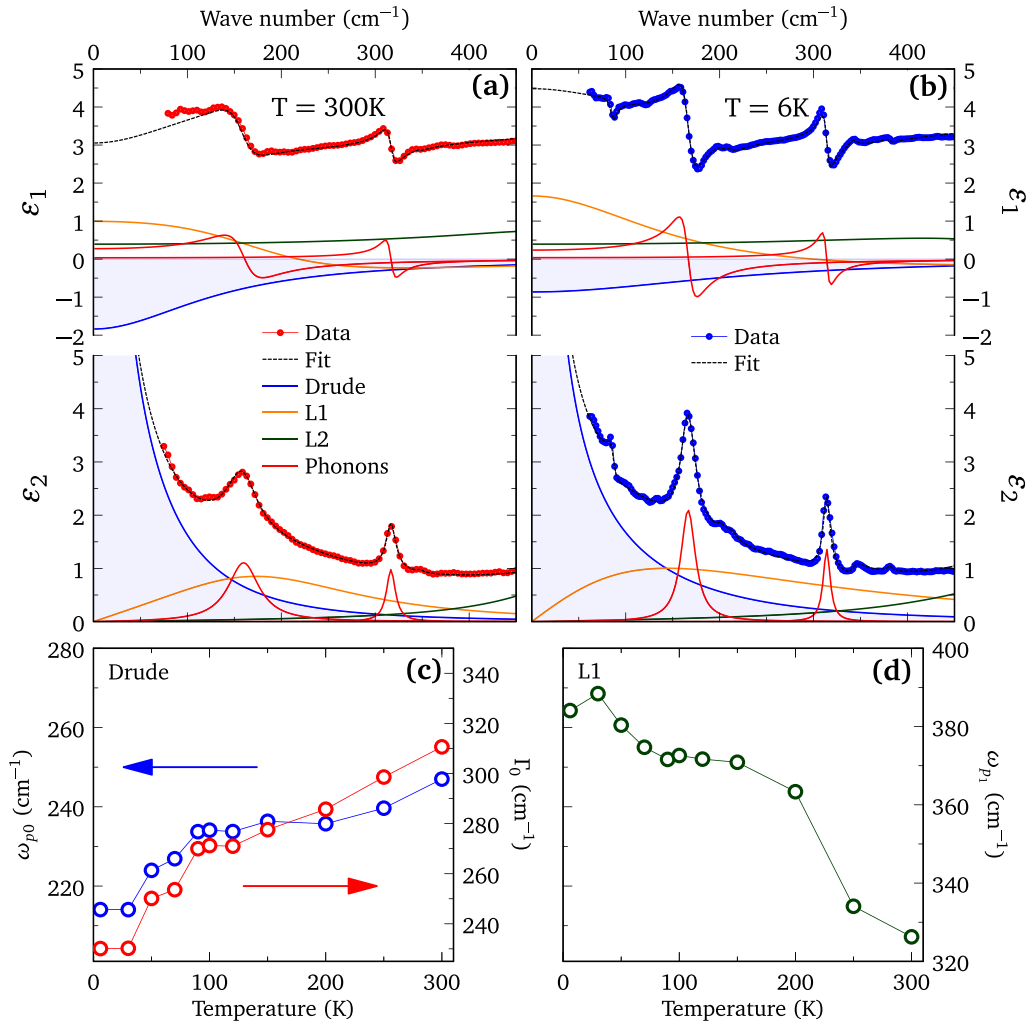


FIG. 5. (a) Spectra at 300 K of the real and imaginary parts of the dielectric function (symbols). The dashed lines show the total fit function and the solid lines show the individual contributions of the Drude response (blue), the low-energy Lorentz oscillators (orange and green), and two phonon modes (red). (b) Corresponding spectra (symbols) and fits (lines) measured at 6 K. (c) Temperature dependence of the obtained fit parameters for the scattering rate, Γ_0 , and the plasma frequency, ω_{p0} , of the Drude peak and (d) of the plasma frequency of the low-energy Lorentz oscillator, ω_{p1} .

in Fig. 6(b). The values have been obtained at two different fixed values of the current density, J , as well as from the I - V curves, taking into account the slope of the branch of the I - V curve measured in the low current range. The resistivity behavior is non-Ohmic, with features that are correlated with the current density. Generally, $\rho(T)$ decreases as T is lowered from 300 K [except at $J = 2.21$ A/cm² where $\rho(T)$ first increases to about 200 K before it decreases], saturating around 30 K and then upturning below 30 K. The low-temperature upturn of $\rho(T)$ becomes more pronounced as the sourced current density is increased. Nevertheless, it is also evident in the curve derived from the I - V characteristics [Fig. 6(b)]. The largest changes in the resistivity have been detected at the highest current density ($J = 2.21$ A/cm²), where $\rho(T)$ exhibits a broad, bell shaped maximum centered around 200 K that closely resembles the behavior shown in Fig. 6(a). A bell shaped resistivity as a function of temperature has been also obtained in a previous study by some of the authors on KPT electrical transport properties in Ref. [41]. The values of $\rho(T)$ derived from the IR spectra are of the same order of magnitude

as those of the electrical measurements at high currents of $J = 1.32$ and 2.21 A/cm² and about one order of magnitude higher than those derived from the I - V curves measured at fixed T [Figs. 6(a) and 6(b)].

These observations seem compatible with the scenario of a spatially inhomogeneous conductivity with conducting patches that are embedded in a matrix of materials that is less conducting. Here, the transport measurements at low current probe primarily the conducting filaments whereas, at a higher current, they are more representative of the averaged conductivity (similar to the infrared data). The temperature-dependent dc resistivity deduced from the IR spectra exhibits some features that are also detected in the electrical transport data at high J value, such as the broad maximum around 200 K and the low- T upturn.

It is worthwhile noting that the low- T upturn of $\rho(T)$ detected by IR below 75 K occurs at a somewhat lower T than that of the suppression of the plasma frequency and the scattering rate in Fig. 5(c). This is due to a partial compensation of the effects of the reduced plasma frequency and scattering

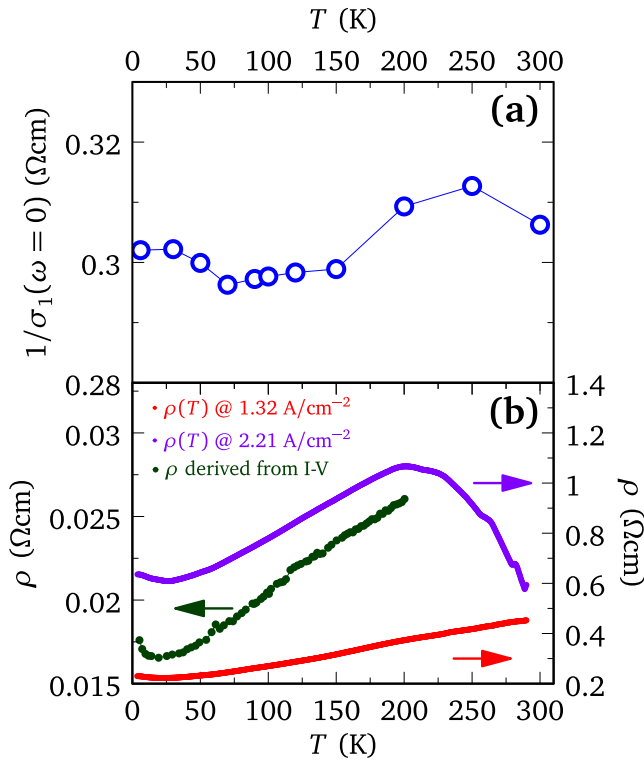


FIG. 6. (a) T dependence of the inverse of the dc conductivity of a K_3p -terphenyl sample, derived from a fit of the IR spectra (extrapolated at $\omega = 0$). (b) Electrical resistivity of a twin sample measured with sourcing current pulses of $J = 1.32 \text{ A/cm}^2$ (red points) and $J = 2.21 \text{ A/cm}^2$ (violet points). Also shown are data derived from the slope of the low current range branch of the I - V curve (dark green points).

rate on the derived value of the dc resistivity. Irrespective of these minor differences, the low- T upturn of $\rho(T)$ appears to be a feature that is common to the transport and infrared data and thus intrinsic to the charge dynamics. In particular, the suppression of the spectral weight of the Drude response below 90 K and the related spectral weight gain of the L_1 band around 220 cm^{-1} in the infrared spectra is indicative of weak localization of some of the charge carriers. Notably, it is inconsistent with the formation of a macroscopic superconducting state for which the missing spectral weight would be redshifted and give rise to a delta function at the origin, that accounts for the loss-free response of the superconducting condensate. The infrared spectra are therefore in contradiction with the scenario that a macroscopic superconducting state develops below 90 K in our K_3p -terphenyl sample. On the other hand, they do not exclude the possibility of a filamentary superconducting state in a small volume fraction of the sample, well below the threshold for percolation. In this context, we note that low-dimensional structures in the form of interconnected filaments have indeed been proposed as a source of amplification of superconductivity by shape resonance effects in Ref. [72]. The plasmonic effects related to a spatial confinement of the superconducting condensate could indeed give rise to a plasmonic mode that is centered at finite frequency [65,73]. The formation of such a plasmonic feature thus could possibly explain the blueshift of some of

the spectral weight of the Drude peak to the L_1 mode that sets in below 90 K.

VI. DISCUSSION AND OUTLOOK

In summary, with infrared ellipsometry we have studied the electronic response of a polycrystalline sample of K_3p -terphenyl. For this purpose we have mounted the sample, that decomposes rapidly under humid ambient conditions, inside a glovebox under dry and inert argon gas atmosphere inside a cell with windows for optical measurements that can be sealed against the ambient. The measured spectra of the electronic conductivity are governed by two pronounced Lorentzian bands with maxima around 4000 and $12\,000 \text{ cm}^{-1}$. Based on the comparison with calculations using a Hückel model, these bands have been assigned to intramolecular excitations of the π electrons of the anionic p -terphenyl molecules. Some discrepancies between experiment and theory, in particular, with respect to the relative spectral weights of these bands, can be explained if the molecules contain less than the nominal three π electrons (but still more than two), in agreement with an effective number of K atoms per p -terphenyl molecule lower than 3 detected experimentally [41]. The corresponding intermolecular excitations give rise to a very weak Drude peak at the origin and most likely also to a weak Lorentzian band around 220 cm^{-1} . The dc resistivity (inverse conductivity) derived from the Drude response is consistent with the behavior of the dc resistivity from electrical transport measured at high current density. As the temperature is reduced below 300 K the plasma frequency and the width of this Drude peak exhibit a gradual decrease that is anomalously enhanced below about 90 K. The related missing spectral weight of the Drude peak at low temperature is blueshifted toward higher energy where it increases the spectral weight of the band at 220 cm^{-1} . Such a blueshift of low-energy spectral weight is not uncommon for such low-dimensional organic conductors for which the carriers tend to get weakly localized as temperature decreases. It certainly contradicts the behavior expected for a bulklike superconductor for which the missing spectral weight of the Drude peak should be redshifted to a delta function at the origin that accounts for the loss-free response of the superconducting condensate. Nevertheless, the infrared data are not necessarily incompatible with a spatially inhomogeneous superconducting state with a volume fraction well below the percolation limit for which the confinement of the superconducting condensate might result in a plasmonic resonance at finite frequency.

ACKNOWLEDGMENTS

Work at University of Fribourg was supported by the Swiss National Science Foundation (SNSF) by Grant No. 200020-172611. We thank M. Andrey from the mechanical workshop at UniFr for designing and building the optical cell, and Changming Yue for helpful discussions.

APPENDIX: HÜCKEL THEORY FOR K_xp -TERPHENYL

In this Appendix we use Hückel theory to calculate the equilibrium structure, the electronic energy levels, and the op-

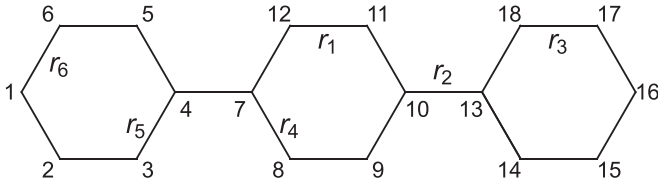


FIG. 7. Structure of *p*-terphenyl and numbering of π orbitals and bond lengths.

tical absorbption for a *p*-terphenyl molecule. The bond lengths r_{ij} between neighboring sites i and j are assumed to remain close to an average value r_0 . We write

$$r_{ij} = r_0 + u_{ij} \quad (\text{A1})$$

and expand the hopping amplitudes as

$$t(r_{ij}) = t_0 - \alpha u_{ij}, \quad (\text{A2})$$

where t_0 is the value at r_0 . The Hamiltonian reads

$$H = \frac{K}{2} \sum_{\langle i,j \rangle} u_{ij}^2 - \sum_{\langle i,j \rangle \sigma} (t_0 - \alpha u_{ij}) (c_{i\sigma}^\dagger c_{j\sigma} + c_{j\sigma}^\dagger c_{i\sigma}) - 2\alpha p_0 \sum_{\langle i,j \rangle} u_{ij}, \quad (\text{A3})$$

where the operators $c_{i\sigma}^\dagger$ ($c_{i\sigma}$) create (annihilate) π electrons at site i with spin σ . The first term is the elastic energy, the second term describes hopping of π electrons between neighboring sites, and the third term fixes the average bond length to r_0 . The quantity p_0 is the average expectation value of the bond order operator

$$p_{ij} = \frac{1}{2} \sum_{\sigma} (c_{i\sigma}^\dagger c_{j\sigma} + c_{j\sigma}^\dagger c_{i\sigma}). \quad (\text{A4})$$

The derivatives of the ground state energy

$$\frac{\partial}{\partial u_{ij}} \langle H \rangle = K u_{ij} + 2\alpha (\langle p_{ij} \rangle - p_0) \quad (\text{A5})$$

vanish at the energy minimum, where one obtains the linear relation

$$u_{ij} = -\frac{2\alpha}{K} (\langle p_{ij} \rangle - p_0). \quad (\text{A6})$$

For systems such as benzene $\langle p_{ij} \rangle$ is the same for all bonds and equal to p_0 , therefore u_{ij} vanishes on all bonds, as it should. For terphenyl $\langle p_{ij} \rangle$ is not constant and therefore the bond lengths are not all equal. Equation (9) can also be used to relate two different systems with similar bond orders, such as benzene and graphene. In fact, an essentially linear function is obtained if we plot the average bond orders of different systems versus their average bond lengths [74]. From the slope of these data one can deduce a value $\alpha/K \approx 0.1 \text{ \AA}$.

We assume the molecule to be planar and symmetric with respect to reflections σ_x and σ_y by the long and short axes, respectively. It follows that there can only be six different bond lengths r_i , $i = 1, \dots, 6$, as illustrated in Fig. 7. We now choose a basis of states which are symmetric or antisymmetric with respect to the two reflection operators, in terms of superpositions of (orthogonalized) π orbitals $|i\rangle$, $i = 1, \dots, 18$.

1. Symmetry-adapted basis

There are six linearly independent states which are even with respect to both σ_x and σ_y and we choose them as (*g* for gerade)

$$\begin{aligned} |gg\rangle_1 &= \frac{1}{2}(|2\rangle + |6\rangle + |15\rangle + |17\rangle), \\ |gg\rangle_2 &= \frac{1}{2}(|3\rangle + |5\rangle + |14\rangle + |18\rangle), \\ |gg\rangle_3 &= \frac{1}{2}(|8\rangle + |9\rangle + |11\rangle + |12\rangle), \\ |gg\rangle_4 &= \frac{1}{\sqrt{2}}(|1\rangle + |16\rangle), \\ |gg\rangle_5 &= \frac{1}{\sqrt{2}}(|4\rangle + |13\rangle), \\ |gg\rangle_6 &= \frac{1}{\sqrt{2}}(|7\rangle + |10\rangle). \end{aligned} \quad (\text{A7})$$

There are also six different states which are even with respect to σ_x and odd with respect to σ_y , namely (*u* for ungerade),

$$\begin{aligned} |gu\rangle_1 &= \frac{1}{2}(|2\rangle + |6\rangle - |15\rangle - |17\rangle), \\ |gu\rangle_2 &= \frac{1}{2}(|3\rangle + |5\rangle - |14\rangle - |18\rangle), \\ |gu\rangle_3 &= \frac{1}{2}(|8\rangle - |9\rangle - |11\rangle + |12\rangle), \\ |gu\rangle_4 &= \frac{1}{\sqrt{2}}(|1\rangle - |16\rangle), \\ |gu\rangle_5 &= \frac{1}{\sqrt{2}}(|4\rangle - |13\rangle), \\ |gu\rangle_6 &= \frac{1}{\sqrt{2}}(|7\rangle - |10\rangle). \end{aligned} \quad (\text{A8})$$

Three states are odd with respect to σ_x and even with respect to σ_y :

$$\begin{aligned} |ug\rangle_1 &= \frac{1}{2}(|2\rangle - |6\rangle + |15\rangle - |17\rangle), \\ |ug\rangle_2 &= \frac{1}{2}(|3\rangle - |5\rangle + |14\rangle - |18\rangle), \\ |ug\rangle_3 &= \frac{1}{2}(|8\rangle + |9\rangle - |11\rangle - |12\rangle). \end{aligned} \quad (\text{A9})$$

Finally, three states are odd with respect to both reflections:

$$\begin{aligned} |uu\rangle_1 &= \frac{1}{2}(|2\rangle - |6\rangle - |15\rangle + |17\rangle), \\ |uu\rangle_2 &= \frac{1}{2}(|3\rangle - |5\rangle - |14\rangle + |18\rangle), \\ |uu\rangle_3 &= \frac{1}{2}(|8\rangle - |9\rangle + |11\rangle - |12\rangle). \end{aligned} \quad (\text{A10})$$

2. Energy levels and equilibrium bond lengths

To find the ground state of the Hamiltonian (6) we have to diagonalize the electronic part for hopping parameters $t_i := t(r_i)$, where the bond lengths r_i can have six different values. In the basis constructed above the Hamiltonian is block

TABLE III. Equilibrium bond lengths (\AA), average bond orders p_0 , and ground state energies E_0 (eV) for different doping levels, according to Hückel theory.

x	r_1	r_2	r_3	r_4	r_5	r_6	p_0	E_0
0	1.387	1.454	1.390	1.402	1.400	1.393	0.619	-71.86
1	1.376	1.434	1.385	1.419	1.413	1.399	0.605	-69.81
2	1.365	1.414	1.380	1.437	1.425	1.404	0.590	-67.89
3	1.373	1.415	1.373	1.435	1.440	1.419	0.565	-64.59
4	1.381	1.417	1.365	1.432	1.456	1.433	0.540	-61.41

diagonal with two 6×6 blocks

$$\begin{pmatrix} 0 & -t_3 & 0 & -\sqrt{2}t_6 & 0 & 0 \\ -t_3 & 0 & 0 & 0 & -\sqrt{2}t_5 & 0 \\ 0 & 0 & -st_1 & 0 & 0 & -\sqrt{2}t_4 \\ -\sqrt{2}t_6 & 0 & 0 & 0 & 0 & 0 \\ 0 & -\sqrt{2}t_5 & 0 & 0 & 0 & -t_2 \\ 0 & 0 & -\sqrt{2}t_4 & 0 & -t_2 & 0 \end{pmatrix} \quad (\text{A11})$$

for the gg and gu sectors (with $s = +1$ in the gg sector and -1 in the gu sector), and two 3×3 blocks

$$\begin{pmatrix} 0 & -t_3 & 0 \\ -t_3 & 0 & 0 \\ 0 & 0 & -st_1 \end{pmatrix} \quad (\text{A12})$$

for the other two symmetries (with $s = +1$ in the ug sector and -1 in the uu sector). The 3×3 matrices are easily diagonalized. There are two nondegenerate levels, one at $-t_1$ with gu symmetry and one at $+t_1$ with uu symmetry, and two doubly degenerate levels at $\pm t_3$.

We discuss first the (hypothetical) case of equal bond lengths, i.e., $t_i = t_0$, $i = 1, \dots, 6$. The eigenvalues for the ug and uu sectors are now at $\pm t_0$. Two eigenvectors at $+t_0$ have uu symmetry and one has ug symmetry, while two eigenvectors at $-t_0$ have ug symmetry and one has uu symmetry. The eigenvalue equations for the gg and gu sectors read

$$(E + st_0)(E^5 - 8t_0^2E^3 + 2st_0^3E^2 + 15t_0^4E - 8st_0^5) = 0. \quad (\text{A13})$$

Therefore we obtain an additional eigenvector at $+t_0$, with gu symmetry, and one at $-t_0$, with gg symmetry. It follows that the levels at $\pm t_0$ are fourfold degenerate, as illustrated in Fig. 4. Only one positive eigenvalue, of gg symmetry, is below t_0 , at $0.592\ 64\ t_0$.

To determine the equilibrium bond lengths we use parameter values $t_0 = 2.9\text{ eV}$, $K = 46\text{ eV \AA}^{-2}$, and $\alpha = 4.5\text{ eV \AA}^{-1}$, in line with Kakitani's analysis of vibrational and electronic properties of small organic molecules [75]. The values of p_0 are determined for equal bond lengths $r_{ij} = r_0$ and r_0 is related to p_0 as $r_0 = (1.525 - 0.2p_0)\text{ \AA}$, in agreement with bond orders and bond lengths of benzene and graphene ($p_0 = \frac{2}{3}$ and $r_0 = 1.39\text{ \AA}$ for benzene and $p_0 = 0.525$ and $r_0 = 1.42\text{ \AA}$ for graphene). The bond lengths obtained by minimizing the total energy for different doping levels are given in Table III.

TABLE IV. Equilibrium bond lengths (\AA) for different doping levels, according to Ref. [76].

x	r_1	r_2	r_3	r_4	r_5	r_6
0	1.390	1.484	1.392	1.402	1.403	1.394
1	1.378	1.450	1.387	1.427	1.427	1.402
2	1.372	1.418	1.382	1.447	1.451	1.414

The numbers agree surprisingly well with results of DFT calculations (Table IV).

The energy levels between 0 and 3.2 eV (which are relevant for the IR absorption) are listed in Table V. For $x = 0$ all these levels are unoccupied. For $x = 1$ and 2 the gg level is, respectively, singly and doubly occupied. Correspondingly, the energy level is lowered substantially. A similar polaronic effect is seen if the gu level is occupied, i.e., from $x = 2$ to 3. For $x = 4$ the gg and gu levels are both doubly occupied.

3. Optical transitions

We now use the Hückel model for treating optical transitions between molecular orbitals. In first quantization the electronic part of the Hamiltonian is

$$H_e = - \sum_{i,j} t_{ij} |i\rangle \langle j|, \quad (\text{A14})$$

where t_{ij} is only finite if the sites i and j are nearest neighbors. In the spirit of tight-binding theory we define the velocity operator as the time derivative of the position operator

$$\mathbf{R} := \sum_i \mathbf{R}_i |i\rangle \langle i|, \quad (\text{A15})$$

where \mathbf{R}_i is the position of the i th atom in the molecule, i.e.,

$$\mathbf{v} = \frac{i}{\hbar} [H, \mathbf{R}] = \frac{i}{\hbar} \sum_{i,j} (\mathbf{R}_i - \mathbf{R}_j) t_{ij} |i\rangle \langle j|. \quad (\text{A16})$$

If intermolecular transitions are neglected, the conductivity is just that of a single molecule multiplied by the number N_0 of molecules per unit volume. Linear-response theory then implies [77]

$$\sigma_{1,\alpha\alpha}(\omega) = \frac{N_0 \pi e^2}{\hbar \omega} \sum_{\mu,\nu} |\langle \mu | v_\alpha | \nu \rangle|^2 \delta(\omega - \omega_{\nu\mu}), \quad (\text{A17})$$

TABLE V. Lowest positive energy eigenvalues (in eV for $t_0 = 2.9\text{ eV}$) for the Hückel model of K_xp -terphenyl. The numbers of the first row have been calculated for equal bond lengths, and the others have been calculated for optimized geometries.

	gg	gu	$uu^{(1)}$	ug	$uu^{(2)}$
$r_i = r_0$	1.719	2.900	2.900	2.900	2.900
$x = 0$	1.783	2.910	2.945	2.945	2.956
$x = 1$	1.658	2.865	2.967	2.967	3.006
$x = 2$	1.538	2.826	2.987	2.987	3.056
$x = 3$	1.501	2.733	3.020	3.023	3.023
$x = 4$	1.464	2.641	2.984	3.058	3.058

where $\alpha = x, y$ is the polarization and $\hbar\omega_{v\mu} = E_v - E_\mu$ is the transition energy between occupied states $|\mu\rangle$ and unoccupied states $|\nu\rangle$ (the labels μ and ν include spin).

This approach has been applied before for polyacetylene [78] using a constant nearest-neighbor hopping amplitude t_0 in the velocity operator. Later it was shown that the length dependence of t_{ij} produces correction terms, which however are small [79]. They will be neglected here.

It is straightforward to calculate the matrix elements between the different orbitals. We consider the levels of Table V for $x = 3$, for which the nonvanishing matrix elements are

$$\langle gg|\mathbf{v}|gu\rangle = -0.3951 i \frac{tr_0}{\hbar} \mathbf{e}_x, \quad (\text{A18})$$

$$\langle gg|\mathbf{v}|ug\rangle = -0.1533 i \frac{tr_0}{\hbar} \mathbf{e}_y, \quad (\text{A19})$$

$$\langle gu|\mathbf{v}|uu\rangle^{(1)} = -0.4670 i \frac{tr_0}{\hbar} \mathbf{e}_y, \quad (\text{A20})$$

$$\langle gu|\mathbf{v}|uu\rangle^{(2)} = -0.5001 i \frac{tr_0}{\hbar} \mathbf{e}_y, \quad (\text{A21})$$

where \mathbf{e}_x and \mathbf{e}_y are unit vectors in the direction of the long and short axis, respectively. The polarization dependence reflects the symmetry of the molecular orbitals.

The spectral weight for the radiative transition $\mu \rightarrow \nu$ with α -polarized light is given by

$$\int_0^\infty d\omega \sigma_{1,\alpha\alpha}^{(\mu \rightarrow \nu)} = \frac{N_0 \pi e^2}{\hbar \omega_{v\mu}} |\langle \mu | v_\alpha | \nu \rangle|^2. \quad (\text{A22})$$

To obtain the average values of Table II one has to sum over the polarization components and divide the result by 3. Moreover the spin gives a factor of 2 for the $gg \rightarrow ug$

transition. In the above analysis we have omitted the transition from the gu level (at 2.7 to 3 eV) to the second gg level (at 4 eV) because its intensity is about 100 times smaller than the other transitions in the same energy range.

4. Doping

In the neutral state of the p -terphenyl molecule (18 π electrons) all negative energy levels are filled. To describe how doping proceeds in a system of N (uncoupled) molecules it is sufficient to consider $N = 2$. A single additional electron occupies the lowest available level of one of the two molecules. This costs an energy $E_0(1) - E_0(0)$, where $E_0(x)$ is the ground state energy of a molecule for x added electrons, as listed in Table III. One would naively expect that a second electron would be added to the other molecule, but another option is to add it to the same, with an energy cost $E_0(2) - E_0(1)$. The numbers of Table III show that the second choice requires less energy, explicitly

$$E_0(2) - 2E_0(1) + E_0(0) = -0.13 \text{ eV}. \quad (\text{A23})$$

We can also say that the state of two singly charged molecules is unstable with respect to a “phase separation” into a neutral and a doubly charged molecule. The same arguments show that two molecules with $x = 3$ have a higher total energy than one with $x = 4$ and one with $x = 2$, because

$$E_0(4) - 2E_0(3) + E_0(2) = -0.12 \text{ eV}. \quad (\text{A24})$$

Therefore according to Hückel’s theory doping proceeds by adding electrons pairwise (by producing bipolarons instead of polarons).

- [1] J. Ferraris, D. O. Cowan, V. Walatka, and J. H. Perlstein, Electron transfer in a new highly conducting donor-acceptor complex, *J. Am. Chem. Soc.* **95**, 948 (1973).
- [2] L. B. Coleman, M. J. Cohen, D. J. Sandman, F. G. Yamagishi, A. F. Garito, and A. J. Heeger, Superconducting fluctuations and the Peierls instability in an organic solid, *Solid State Commun.* **12**, 1125 (1973).
- [3] J. B. Torrance, The difference between metallic and insulating salts of tetracyanoquinodimethane (TCNQ): How to design an organic metal, *Acc. Chem. Res.* **12**, 79 (1979).
- [4] K. Bechgaard, C. S. Jacobsen, K. Mortensen, H. J. Pedersen, and N. Thorup, The properties of five highly conducting salts: (TMTSF)₂X, X = PF₆[−], AsF₆[−], SbF₆[−], BF₄[−] and NO₃[−], derived from tetramethyltetraselenafulvalene (TMTSF), *Solid State Commun.* **33**, 1119 (1980).
- [5] D. Jérôme, Organic conductors: From charge density wave TTF-TCNQ to superconducting (TMTSF)₂PF₆, *Chem. Rev.* **104**, 5565 (2004).
- [6] D. Jérôme, A. Mazaud, M. Ribault, and K. Bechgaard, Superconductivity in a synthetic organic conductor (TMTSF)₂ PF₆, *J. Phys. Lett.* **41**, 95 (1980).
- [7] S. S. P. Parkin, M. Ribault, D. Jérôme, and K. Bechgaard, Superconductivity in the family of organic salts based on the tetramethyltetraselenafulvalene (TMTSF) molecule (TMTSF)₂ X (X= ClO₄, PF₆, AsF₆, SbF₆, TaF₆), *J. Phys. C: Solid State Phys.* **14**, 5305 (1981).
- [8] W. A. Little, Possibility of synthesizing an organic superconductor, *Phys. Rev.* **134**, A1416 (1964).
- [9] J. M. Williams, A. J. Schultz, U. Geiser, K. D. Carlson, A. M. Kini, H. G. Wang, W.-K. Kwok, M.-H. Whangbo, and J. E. Schirber, Organic superconductors – new benchmarks, *Science* **252**, 1501 (1991).
- [10] H. Taniguchi, M. Miyashita, K. Uchiyama, K. Satoh, N. Môri, H. Okamoto, K. Miyagawa, K. Kanoda, M. Hedo, and Y. Uwatoko, Superconductivity at 14.2 K in layered organics under extreme pressure, *J. Phys. Soc. Jpn.* **72**, 468 (2003).
- [11] B. J. Powell and R. H. McKenzie, Quantum frustration in organic Mott insulators: From spin liquids to unconventional superconductors, *Rep. Prog. Phys.* **74**, 056501 (2011).
- [12] A. Ardavan, S. Brown, S. Kagoshima, K. Kanoda, K. Kuroki, H. Mori, M. Ogata, S. Uji, and J. Wosnitzer, Recent topics of organic superconductors, *J. Phys. Soc. Jpn.* **81**, 011004 (2012).
- [13] M. Dressel and N. Drichko, Optical properties of two-dimensional organic conductors: Signatures of charge ordering and correlation effects, *Chem. Rev.* **104**, 5689 (2004).
- [14] L. Forró and L. Mihály, Electronic properties of doped fullerenes, *Rep. Prog. Phys.* **64**, 649 (2001).
- [15] M. S. Dresselhaus, G. Dresselhaus, and P. C. Eklund, *Science of Fullerenes and Carbon Nanotubes* (Elsevier, Amsterdam, 1996).
- [16] L. Degiorgi, Fullerenes and carbon derivatives: From insulators to superconductors, *Adv. Phys.* **47**, 207 (1998).

- [17] A. F. Hebard, M. J. Rosseinsky, R. C. Haddon, D. W. Murphy, S. H. Glarum, T. T. M. Palstra, A. P. Ramirez, and A. R. Kortan, Superconductivity at 18 K in potassium-doped C_{60} , *Nature (London)* **350**, 600 (1991).
- [18] Y. Takabayashi, A. Y. Ganin, P. Jeglič, D. Arčon, T. Takano, Y. Iwasa, Y. Ohishi, M. Takata, N. Takeshita, K. Prassides, and M. J. Rosseinsky, The disorder-free non-BCS superconductor Cs_3C_{60} emerges from an antiferromagnetic insulator parent state, *Science* **323**, 1585 (2009).
- [19] O. Gunnarsson, Superconductivity in fullerides, *Rev. Mod. Phys.* **69**, 575 (1997).
- [20] M. Capone, M. Fabrizio, C. Castellani, and E. Tosatti, Colloquium: Modeling the unconventional superconducting properties of expanded A_3C_{60} fullerides, *Rev. Mod. Phys.* **81**, 943 (2009).
- [21] R.-S. Wang, D. Peng, L.-N. Zong, L.-C. Chen, and X.-J. Chen, Variation of the critical temperature with the lattice parameter in K_3C_{60} , *Carbon* **199**, 181 (2022).
- [22] P. J. Benning, F. Stepniak, and J. H. Weaver, Electron-diffraction and photoelectron-spectroscopy studies of fullerene and alkali-metal fulleride films, *Phys. Rev. B* **48**, 9086 (1993).
- [23] T. Yildirim, L. Barbedette, J. E. Fischer, C. L. Lin, J. Robert, P. Petit, and T. T. M. Palstra, T_c vs Carrier Concentration in Cubic Fulleride Superconductors, *Phys. Rev. Lett.* **77**, 167 (1996).
- [24] M.-Q. Ren, S. Han, S.-Z. Wang, J.-Q. Fan, C.-L. Song, X.-C. Ma, and Q.-K. Xue, Direct Observation of Full-Gap Superconductivity and Pseudogap in Two-Dimensional Fullerides, *Phys. Rev. Lett.* **124**, 187001 (2020).
- [25] L.-N. Zong, R.-S. Wang, D. Peng, and X.-J. Chen, Superconductivity in nonstoichiometric rubidium-doped C_{60} , *J. Phys. Chem. C* **126**, 2912 (2022).
- [26] R. Mitsuhashi, Y. Suzuki, Y. Yamanari, H. Mitamura, T. Kambe, N. Ikeda, H. Okamoto, A. Fujiwara, M. Yamaji, N. Kawasaki, Y. Maniwa, and Y. Kubozono, Superconductivity in alkali-metal-doped picene, *Nature (London)* **464**, 76 (2010).
- [27] Y. Kubozono, R. Eguchi, H. Goto, S. Hamao, T. Kambe, T. Terao, S. Nishiyama, L. Zheng, X. Miao, and H. Okamoto, Recent progress on carbon-based superconductors, *J. Phys.: Condens. Matter* **28**, 334001 (2016).
- [28] X. F. Wang, R. H. Liu, Z. Gui, Y. L. Xie, Y. J. Yan, J. J. Ying, X. G. Luo, and X. H. Chen, Superconductivity at 5 K in alkali-metal-doped phenanthrene, *Nat. Commun.* **2**, 507 (2011).
- [29] M. Xue, T. Cao, D. Wang, Y. Wu, H. Yang, X. Dong, J. He, F. Li, and G. F. Chen, Superconductivity above 30 K in alkali-metal-doped hydrocarbon, *Sci. Rep.* **2**, 389 (2012).
- [30] T. Nakagawa, Z. Yuan, J. Zhang, K. Yussenko, C. Drathen, Q. Liu, S. Margadonna, and C. Jin, Structure and magnetic property of potassium intercalated pentacene: Observation of superconducting phase in $K_xC_{22}H_{14}$, *J. Phys.: Condens. Matter* **28**, 484001 (2016).
- [31] S. Heguri, M. Kobayashi, and K. Tanigaki, Questioning the existence of superconducting potassium doped phases for aromatic hydrocarbons, *Phys. Rev. B* **92**, 014502 (2015).
- [32] G. Huang, G.-H. Zhong, R.-S. Wang, J.-X. Han, H.-Q. Lin, and X.-J. Chen, Superconductivity and phase stability of potassium-doped p-quinquephenyl, *Carbon* **143**, 837 (2019).
- [33] J.-F. Yan, G.-H. Zhong, R.-S. Wang, K. Zhang, H.-Q. Lin, and X.-J. Chen, Superconductivity and phase stability of potassium-intercalated p-quaterphenyl, *J. Phys. Chem. Lett.* **10**, 40 (2019).
- [34] G.-H. Zhong, D.-Y. Yang, K. Zhang, R.-S. Wang, C. Zhang, H.-Q. Lin, and X.-J. Chen, Superconductivity and phase stability of potassium-doped biphenyl, *Phys. Chem. Chem. Phys.* **20**, 25217 (2018).
- [35] R.-S. Wang, Y. Gao, Z.-B. Huang, and X.-J. Chen, Superconductivity at 43 K in a single C-C bond linked terphenyl, *arXiv:1703.06641*.
- [36] R.-S. Wang, Y. Gao, Z.-B. Huang, and X.-J. Chen, Superconductivity above 120 Kelvin in a chain link molecule, *arXiv:1703.06641*.
- [37] P. Neha, A. Bhardwaj, V. Sahu, and S. Patnaik, Facile synthesis of potassium intercalated p-terphenyl and signatures of a possible high T_c phase, *Physica C: Superconductivity Appl.* **554**, 1 (2018).
- [38] W. Liu, H. Lin, R. Kang, X. Zhu, Y. Zhang, S. Zheng, and H.-H. Wen, Magnetization of potassium-doped p-terphenyl and p-quaterphenyl by high-pressure synthesis, *Phys. Rev. B* **96**, 224501 (2017).
- [39] H. Li, X. Zhou, S. Parham, T. Nummy, J. Griffith, K. N. Gordon, E. L. Chronister, and D. S. Dessau, Spectroscopic evidence of low-energy gaps persisting up to 120 K in surface-doped p-terphenyl crystals, *Phys. Rev. B* **100**, 064511 (2019).
- [40] M. Q. Ren, W. Chen, Q. Liu, C. Chen, Y. J. Qiao, Y. J. Chen, G. Zhou, Z. H. Li, T. Zhang, Y. J. Yan, and D. L. Feng, Observation of gapped phases in potassium-doped single-layer p-terphenyl on Au (111), *Phys. Rev. B* **99**, 045417 (2019).
- [41] N. Pinto, C. Di Nicola, A. Trapananti, M. Minicucci, A. Di Cicco, A. Marcelli, A. Bianconi, F. Marchetti, C. Pettinari, and A. Perali, Potassium-doped para-terphenyl: Structure, electrical transport properties and possible signatures of a superconducting transition, *Condensed Matter* **5**, 78 (2020).
- [42] G.-H. Zhong, X.-H. Wang, R.-S. Wang, J.-X. Han, C. Zhang, X.-J. Chen, and H.-Q. Lin, Structural and bonding characteristics of potassium-doped p-terphenyl superconductors, *J. Phys. Chem. C* **122**, 3801 (2018).
- [43] X.-W. Yan, Z. Huang, M. Gao, and C. Zhang, Stable structural phase of potassium-doped p-terphenyl and its semiconducting state, *J. Phys. Chem. C* **122**, 27648 (2018).
- [44] A. Guijarro and J. A. Vergés, Gap opening in the most stable phases of K_3 terphenyl compound, *Mater. Res. Express* **6**, 125111 (2019).
- [45] F. Wooten, Optical properties of solids, *Am. J. Phys.* **41**, 939 (1973).
- [46] M. Dressel and G. Grüner, *Electrodynamics of Solids: Optical Properties of Electrons in Matter* (Cambridge University, New York, 2002).
- [47] H. K. Ng, T. Timusk, D. Jérôme, and K. Bechgaard, Far-infrared spectrum of di-tetramethyltetraselenafulvalene hexafluoroarsenate $[(TMTSF)_2AsF_6]$, *Phys. Rev. B* **32**, 8041 (1985).
- [48] I. Ito, T. Sasaki, N. Yoneyama, N. Kobayashi, N. Hanasaki, H. Tajima, T. Ito, and Y. Iwasa, Infrared optical conductivity and the electronic phase diagram in the organic superconductor κ -(BEDT-TTF) $_2X$, *J. Phys. IV (Proceedings)* **114**, 321 (2004).
- [49] J. Eldridge, K. Kornelsen, H. H. Wang, J. M. Williams, A. Strieby Crouch, and D. Watkins, Infrared optical properties of the 12 K organic superconductor κ -(BEDT-TTF) $_2Cu[N(CN)_2]Br$, *Solid State Commun.* **79**, 583 (1991).
- [50] K. Kornelsen, J. Eldridge, C. Homes, H. H. Wang, and J. Williams, Optical properties of the 10 K organic superconduct-

- tor (BEDT-TTF)₂[Cu(SCN)₂], *Solid State Commun.* **72**, 475 (1989).
- [51] K. Kornelsen, J. E. Eldridge, H. H. Wang, and J. M. Williams, Infrared optical properties of the 10 K organic superconductor (BEDT-TTF)₂[Cu(NCS)₂], *Phys. Rev. B* **44**, 5235 (1991).
- [52] M. Dressel, Electrodynamics of Bechgaard salts: Optical properties of one-dimensional metals, *International Scholarly Research Notices* **2012**, 732973 (2012).
- [53] D. E. Aspnes and A. A. Studna, Dielectric functions and optical parameters of Si, Ge, GaP, GaAs, GaSb, InP, InAs, and InSb from 1.5 to 6.0 eV, *Phys. Rev. B* **27**, 985 (1983).
- [54] E. H. Korte and A. Röseler, Infrared spectroscopic ellipsometry: A tool for characterizing nanometer layers, *Analyst* **123**, 647 (1998).
- [55] M. Schubert, C. Bundesmann, G. Jakopic, H. Maresch, H. Arwin, N.-C. Persson, F. Zhang, and O. Inganäs, Infrared ellipsometry characterization of conducting thin organic films, *Thin Solid Films* **455**, 295 (2004).
- [56] C. Bernhard, J. Humlíček, and B. Keimer, Far-infrared ellipsometry using a synchrotron light source—the dielectric response of the cuprate high T_c superconductors, *Thin Solid Films* **455**, 143 (2004).
- [57] N. Matsumoto, T. Hosokura, T. Nagashima, and M. Hangyo, Measurement of the dielectric constant of thin films by terahertz time-domain spectroscopic ellipsometry, *Opt. Lett.* **36**, 265 (2011).
- [58] C. M. Morris, R. Valdés Aguilar, A. V. Stier, and N. P. Armitage, Polarization modulation time-domain terahertz polarimetry, *Opt. Express* **20**, 12303 (2012).
- [59] P. Marsik, K. Sen, J. Khmaladze, M. Yazdi-Rizi, B. P. Mallett, and C. Bernhard, Terahertz ellipsometry study of the soft mode behavior in ultrathin SrTiO₃ films, *Appl. Phys. Lett.* **108**, 052901 (2016).
- [60] K. Hinrichs, M. Gensch, and N. Esser, Analysis of organic films and interfacial layers by infrared spectroscopic ellipsometry, *Appl. Spectrosc.* **59**, 272A (2005).
- [61] A. Daire, An improved method for differential conductance measurements, Keithley white paper (2005), <https://download.tek.com/document/2687%20Diff.pdf>.
- [62] V. Kumar and A. K. Datta, Vacuum ultraviolet scintillators: Sodium salicylate and *p*-terphenyl, *Appl. Opt.* **18**, 1414 (1979).
- [63] L. Andrushenko, J. Baker, S. Budakovsky, N. Galunov, V. Titov, and I. Yermolenko, Combined detectors based on crystalline *p*-terphenyl for detection of UV-radiation, *Mol. Cryst. Liq. Cryst.* **361**, 293 (2001).
- [64] P. Puschnig, G. Heimel, K. Weinmeier, R. Resel, and C. Ambrosch-Draxl, High pressure studies on the optical and electronic properties of para-terphenyl, *High Press. Res.* **22**, 105 (2002).
- [65] A. H. Sihvola, *Electromagnetic Mixing Formulas and Applications*, Vol. 47, IET Digital Library, 1999.
- [66] E. Hückel, Quantentheoretische Beiträge zum Benzolproblem, *Z. Phys.* **70**, 204 (1931).
- [67] E. Hückel, Quantentheoretische Beiträge zum Problem der aromatischen und ungesättigten Verbindungen, *Z. Phys.* **76**, 628 (1932).
- [68] L. Salem, *Molecular Orbital Theory of Conjugated Systems* (Benjamin, New York, 1966).
- [69] L. Pietronero and S. Strässler, Bond-Length Change as a Tool to Determine Charge Transfer and Electron-Phonon Coupling in Graphite Intercalation Compounds, *Phys. Rev. Lett.* **47**, 593 (1981).
- [70] C. L. Wang, W. Z. Wang, and Z. B. Su, An analytic solution of C₆₀ molecular orbitals, *J. Phys.: Condens. Matter* **5**, 5851 (1993).
- [71] D. Baeriswyl, D. K. Campbell, and S. Mazumdar, An overview of the theory of π -conjugated polymers, *Springer Ser. Solid-State Sci.* **102**, 7 (1992).
- [72] M. V. Mazziotti, A. Valletta, G. Campi, D. Innocenti, A. Perali, and A. Bianconi, Possible Fano resonance for high- T_c multi-gap superconductivity in *p*-Terphenyl doped by K at the Lifshitz transition, *Europhys. Lett.* **118**, 37003 (2017).
- [73] C. N. Wang, P. Marsik, R. Schuster, A. Dubroka, M. Rössle, C. Niedermayer, G. D. Varma, A. F. Wang, X. H. Chen, T. Wolf, and C. Bernhard, Macroscopic phase segregation in superconducting K_{0.73}Fe_{1.67}Se₂ as seen by muon spin rotation and infrared spectroscopy, *Phys. Rev. B* **85**, 214503 (2012).
- [74] D. Baeriswyl, Theoretical aspects of conducting polymers: Electronic structure and defect states, in *Theoretical Aspects of Band Structures and Electronic Properties of Pseudo-One-Dimensional Solids*, edited by H. Kamimura (Reidel, Dordrecht, 1985).
- [75] T. Kakitani, Theoretical study of optical absorption curves of molecules. III: Force constant and bond-bond interaction in conjugated molecules, *Prog. Theor. Phys.* **51**, 656 (1974).
- [76] A. Sakamoto, T. Harada, and N. Tonegawa, A new approach to the spectral study of unstable radicals and ions in solution by the use of an inert gas glovebox system: Observation and analysis of the infrared spectra of the radical anion and dianion of *p*-Terphenyl, *J. Phys. Chem. A* **112**, 1180 (2008).
- [77] M. Lax, Generalized mobility theory, *Phys. Rev.* **109**, 1921 (1958).
- [78] D. Baeriswyl, G. Harbeke, H. Kiess, E. Meier, and W. Meyer, Optical transitions in oriented polyacetylene, *Physica B+C* **117**, 617 (1983).
- [79] F. Gebhard, K. Bott, M. Scheidler, P. Thomas, and S. W. Koch, Optical absorption of non-interacting tight-binding electrons in a Peierls-distorted chain at half band-filling, *Philos. Mag. B* **75**, 1 (1997).